Clim Dyn (2007) 29:575–590
DOI 10.1007/s00382-007-0249-6

Impact of resolving the diurnal cycle in an ocean–atmosphere GCM. Part 1: a diurnally forced OGCM

D. J. Bernie · E. Guilyardi · G. Madec · J. M. Slingo · S. J. Woolnough

Received: 10 November 2006 / Accepted: 21 March 2007 / Published online: 15 May 2007

Abstract The diurnal cycle is a fundamental time scale in the climate system, at which the upper ocean and atmosphere are routinely observed to vary. Current climate models, however, are not configured to resolve the diurnal cycle in the upper ocean or the interaction of the ocean and atmosphere on these time scales. This study examines the diurnal cycle of the tropical upper ocean and its climate impacts. In the present paper, the first of two, a high vertical resolution ocean general circulation model (OGCM), with modified physics, is developed which is able to resolve the diurnal cycle of sea surface temperature (SST) and current variability in the upper ocean. It is then validated against a satellite derived parameterization of diurnal SST variability and in-situ current observations. The model is then used to assess rectification of the intraseasonal SST response to the Madden–Julian oscillation (MJO) by the diurnal cycle of SST. Across the equatorial Indo-Pacific it is found that the diurnal cycle increases the intraseasonal SST response to the MJO by around 20%. In the Pacific, the diurnal cycle also modifies the exchange of momentum between equatorially divergent Ekman currents and the meridionally convergent geostrophic currents beneath, resulting in a 10% increase in the strength of the Ekman cells and equatorial upwelling. How the thermodynamic and dynamical impacts of the diurnal cycle effect the mean state, and variability, of the climate system cannot be fully investigated in the constrained design of ocean-only experiments presented here. The second part of this study, published separately, addresses the climate impacts of the diurnal cycle in the coupled system by coupling the OGCM developed here to an atmosphere general circulation model.

D. J. Bernie · E. Guilyardi · J. M. Slingo · S. J. Woolnough
National Centre for Atmospheric Science - Climate, Department of Meteorology, University of Reading, Reading, UK

D. J. Bernie · E. Guilyardi · G. Madec
Laboratoire d'Océanographie et du Climat, Expérimentation et Approches Numériques, IPSL, Paris, France

D. J. Bernie (✉)
Met Office Hadley Centre, Fitzroy road, Exeter EX1 3PB, UK
e-mail: dan.bernie@metoffice.gov.uk

1 Introduction

1.1 Background

Due to the movement of the earth the climate system is externally forced at three different time scales; precessional, seasonal and diurnal. The climate of the next century is significantly affected by the latter two, but ocean–atmosphere coupling in the current design of general circulation models (GCM) deals only with seasonal variations.

The most prevalent feature of the diurnal cycle of ocean–atmosphere coupling is the diurnal cycle of sea surface temperature (SST). Large areas of the global oceans exhibit a diurnal cycle of SST (Dsst from herein) (Stommel et al. 1969; Anderson et al. 1996; Kawai and Kawamura 2002; Stuart-Menteth et al. 2003; Ward 2006) which have been observed to reach 2–3°C in favorable conditions of high insolation and low winds, where the Dsst is taken as the difference between the the daily maximum and minumim. In large areas of the tropics the

annual mean Dsst is often 0.5–1°C with large spatial variations which reflect the different typical meteorological conditions.

Exchanges of heat, moisture and gases at the surface of the ocean are highly sensitive to surface temperature and so an accurate knowledge of SST is fundamental to accurate calculations of fluxes between the ocean and atmosphere. Over the tropical oceans the atmosphere is typically moist and near saturation, producing a strong sensitivity of atmospheric convection to SST. This relationship between SST and convection is highlighted by Johnson et al. (1999) who note that during TOGA-COARE (Webster and Lukas 1992) there was a strong link between periods of large Dsst (>1°C) in the western Pacific warm pool and the occurrence of a diurnal cycle of cumulus congestus convection. They point out that congestus convection has a diurnal cycle which peaks in the early afternoon, similar to a continental regime, implying that it is forced by the Dsst (i.e., by surface driven instabilities). The presence of the Dsst and the atmospheric diurnal cycle of congestus suggests that, in some regimes, ocean–atmosphere coupling is apparent at diurnal time scales. Furthermore, Slingo et al. (2003) cite the diurnal cycle of congestus during TOGA-COARE as potentially important to the Madden–Julian oscillation (MJO) pointing out that mid-level outflow from congestus phase of convection leads to a moistening of the free troposphere which may act to set a time scale for the deep convection of the active phase of the MJO (c.f. the recharge–discharge theory of Blade and Hartmann 1993).

Bernie et al. (2005) (B05 from herein) examine the role of the diurnal cycle in the ocean–atmosphere coupling of the MJO by examining the oceanic response to the MJO. They use a high resolution 1D vertical mixed layer model to study the intraseasonal SST response to the MJO and demonstrate, for the TOGA-COARE period, that over a third of the intraseasonal SST response to the MJO is accounted for by the rectification of the intraseasonal signal by the Dsst. This effect is due to the modulation of the Dsst by the different phases of the MJO, with a large Dsst during the light wind and high insolation of the convectively suppressed phase of the MJO. During these periods there is also an underlying intraseasonal warming of the mixed layer. They propose that the absence of the diurnal cycle may be the cause of the weak intraseasonal SST response to the MJO in a coupled general circulation model (CGCM) documented by Inness et al. (2003) which does not resolve the diurnal cycle. B05 interpret the implied reduction in intraseasonal SST response in CGCM, due to the lack of a diurnal cycle, as a weakening of the thermodynamical coupling between the ocean and atmosphere on the time scale of the MJO.

The importance of air–sea coupling to the MJO is also supported by its poor respresentation in atmosphere-only general circulation models (AGCM) and its improvement in coupled ocean–atmosphere GCM demonstrated by Inness and Slingo (2003); Rajendran and Kitoh (2006); Woolnough et al. (2007); Zhang et al. (2006), though the results have not always been consistent and improvements often limited. Studies of ocean–atmosphere coupling have also raised other issues. Inness et al. (2003) draw attention to the role of the basic state, particularly the low level winds, and also note that though the variability of surface fluxes associated with the MJO is of a realistic magnitude, in the model they study, the intraseasonal SST response is too small, suggesting that this is due to shortcomings in the representation of the upper ocean.

From the atmospheric perspective the Dsst is similar in its evolution to the diurnal cycle of land temperatures, with peak warming in the afternoon. But, whereas the magnitude of land surface diurnal temperature variability is solely a thermodynamical response to surface heat fluxes, Dsst is a consequence of not only the diurnal cycle of heat fluxes but also of the diurnal cycle of turbulent mixing which is affected by a number of different physical mechanisms in the upper ocean. For clarification a brief overview of the salient features and important physical processes involved in the diurnal cycle in the upper ocean follows.

1.2 Physical processes and features of the diurnal cycle

In the ocean, the turbulent boundary layer (TBL) extends over the depth through which surface driven turbulent mixing can penetrate. It is the diurnal variability of the depth of the TBL that is central to explaining the diurnal cycle in the upper ocean.

At the most basic level, the depth of the TBL represents a balance between vertical turbulent mixing, which weakens stable density stratification, and processes which lead to an increase in density stratification. Destabilization of the water column occurs through negative surface buoyancy fluxes and fluxes of momentum due to wind stress, producing convective and shear driven turbulent mixing, respectively. Stabilization of the water column occurs due to the vertical gradient of short wave radiation absorption and through positive surface buoyancy fluxes (the additional role of biological factors in this stabilisation is discussed in the conclusions). The balance between these effects leads to the following, rather idealized, paradigm of the diurnal cycle (illustrated in Fig. 1).

During the early morning the onset of shortwave radiative heating leads to a rapid shoaling of the TBL. During this time the thinness of the TBL means that it has a lower heat capacity and so the typically positive heat fluxes absorbed over the TBL lead to a rapid increase in temperature. Meanwhile stable stratification builds up

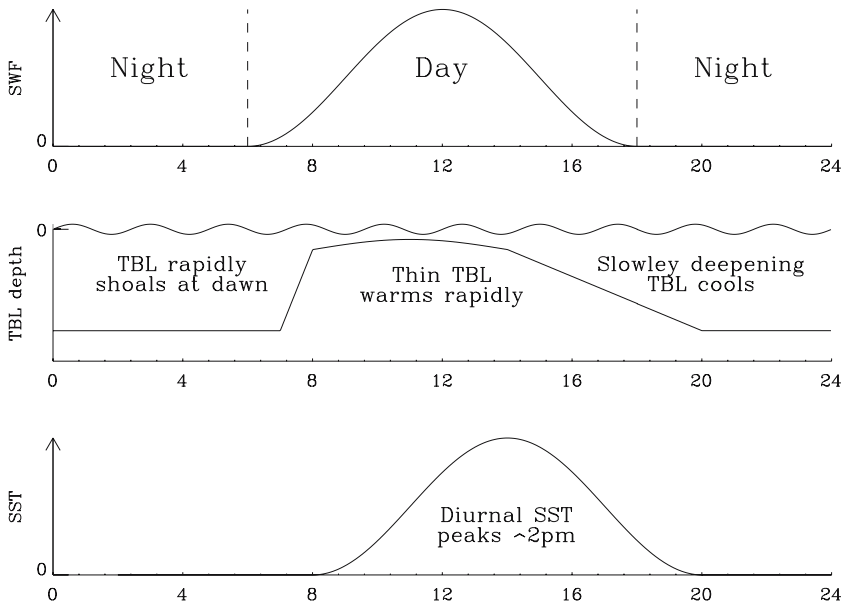

Fig. 1 Schematic showing an idealized diurnal cycle of the upper ocean in terms of short wave fluxes (SWF), turbulent boundary layer depth and sea surface temperature

beneath due to the penetration of short wave fluxes (SWF) through the TBL. The strength of the warming of the TBL depends mainly on the meteorological conditions at the time with larger SWF and lower winds leading to thinner and warmer TBLs, though this may be somewhat compensated by an increase in latent heat fluxes at the surface due to the increased SST. As the day progresses through the afternoon and the sun begins to dip the stabilizing effects of absorption of SWF are reduced causing the TBL to become increasingly dominated by turbulence and deepen. As it does the heat that has accumulated in the TBL during the day is mixed over a greater depth leading to a rapid decrease in temperature (and SST). During the night, the strong surface driven cooling often leads to strong mixing and drives the TBL to its greatest depth. By the following morning, the stratification that had built up below the shallow TBL during the previous day, due to the penetration of SWF, has been removed from above the maximum depth of the nocturnal TBL. This removal of stratification by strong nocturnal mixing leaves a 'clean slate' for the next days diurnal cycle of TBL depth. The stratification below the nocturnal maximum of the TBL, however, remains unaffected. Whether this SWF penetration is significant will depend upon the absorption profile of the SWF and the maximum depth of the nocturnal TBL.

The size of Dsst is therefore dependent not only upon the surface heat fluxes but is also largely determined by the amount of vertical mixing in the upper ocean. Strong mixing from high wind stress results in a decreased Dsst when all other factors are equal.

In addition to the temperature variability, the diurnal variations in the depth of the TBL also have a profound effect upon the diurnal cycle of near surface currents which are somewhat similar to that of the temperature. When the TBL starts to shoal after dawn, surface fluxes of momentum from windstress are contained in a thin layer which accelerates downwind and rotates due to the Coriolis force. As the sun drops and the TBL deepens, the momentum of the TBL is redistributed over a greater depth and the speed of the current decreases as it continues to rotate. By the following morning there is a 'clean slate' for the next day's diurnal cycle. This diurnal cycling of near surface currents has been often observed (e.g., Stommel et al. 1969; Price et al. 1986; Wijffels et al. 1994) and the term 'diurnal jet' is often used to describe this process.

The left hand panels of Fig. 4 show a week long composite of upper ocean currents through the diurnal cycle from the Long Term Upper Ocean Study (LOTUS) mooring (Briscoe and Weller 1984) in a similar fashion to Fig. 9 of Price and Sundermeyer (1999) (PS99 from herein). The data have had the currents at a depth of 50 m removed to account for the geostrophic component. Overlaid as black arrows is the mean current at each depth in which the classical Ekman spiral is evident. The study of PS99 found that the inclusion of the diurnal cycle in various formulations of 1D mixed layer models leads to a flattened mean Ekman spiral which decays faster than it rotates compared to experiments with no diurnal cycle. This resulted in a more realistic mean current profile in their experiment compared to classical Ekman theory.

1.3 Scope of paper

If the diurnal cycle of ocean–atmosphere interaction is important to the climate and its variability then, to make progress using GCMs, it should be properly resolved. To examine if the diurnal cycle of air–sea coupling is indeed important, a model must first be configured to be able to resolve it. This study first develops an OGCM configuration that is able to resolve the diurnal cycle in the upper ocean, particularly Dsst. The impact of the diurnal cycle at different time scales is then addressed.

At intraseasonal time scales, this study addresses the rectification of the SST response to the MJO by the Dsst. Previous results by B05 showed that for a single mooring deployed during TOGA-COARE the Dsst increased the intraseasonal SST response by around a third. This study aims to assess the validity of this finding over a much larger spatial domain of the tropical Indo-Pacific.

Another scientific aim of this study is to examine if there is any impact of the diurnal cycle on the dynamics of the upper ocean. Previous studies of diurnal current variability have exclusively examined diurnal cycle in terms of the impact on mean current profiles at single ocean moorings (e.g., PS99; Wijffels et al. 1994). In this study we examine for the first time the impact of the diurnal cycle on basin scale dynamics, specifically those of the tropical Pacific.

The work presented in this study is performed with the intention of subsequently examining the role of the diurnal cycle in the coupled ocean–atmosphere system. Toward this aim, the present study details the refinement and validation of an ocean GCM which can resolve the diurnal cycle so that it will then be subsequently coupled to an atmospheric GCM. However, the sensitivity tests performed in this work are an important step toward the coupled experiments, as they allow an extraction of the important physical mechanisms at work without the added complication of atmospheric feedbacks.

The structure of the remainder of this paper is as follows: the experimental methodology is detailed in Sect. 2, including a description of the OGCM used. Sects. 3 and 4 provide a validation of the thermal and dynamical modelled diurnal cycle, respectively, detailing refinements made to the model formulation where necessary. The impact of the diurnal cycle on the local intraseasonal SST response to the MJO is given in Sect. 5 and an assessment of the impact of the diurnal cycle on the dynamics of the upper ocean is presented in Sect. 6. A discussion of the results and their implications for the coupled system and future modelling studies are given in Sect. 7.

The impact of the results presented in this paper on the mean state and variability of the coupled ocean–atmosphere system are presented in part 2 of this study (Bernie et al. 2007).

2 Methodology

2.1 The OPA OGCM

The OGCM used in this study is version 8.2 of the OPA (Océan PArallélisé) OGCM (Madec et al. 1998) developed at LOCEAN (formerly LODYC), Paris. OPA is based on the primitive equations (including potential temperature, salinity and horizontal currents), solved by finite difference schemes. Vertical mixing is modelled with a prognostic turbulent kinetic energy (TKE) scheme (Blanke and Delecluse 1993) and solar radiation penetrates the ocean with a three band exponential absorption following Morel and Antoine (1994) for a globally constant chlorophyll concentration of 0.05 mg m^{-3}. A non-penetrative convective adjustment scheme is used to remove instability in the water column (Madec et al. 1991). Isopycnal diffusion and an eddy induced velocity with time–space variable coefficients are also used. The configuration used throughout this study is known as ORCA2 which has a tripolar horizontal curvilinear mesh used to overcome the north pole singularity found for geographical meshes and which is global in extent. The configuration has a nominal resolution of 2°. It is based on a 2° Mercator mesh, (i.e., variation of meridian scale factor as co-sinus of the latitude). In the northern hemisphere the mesh has two poles so that the ratio of anisotropy is nearly one everywhere. The mean grid spacing is about 2/3 of the nominal value. The zonal resolution is 2° while the meridional resolution varies from 2° in the extra-tropics to 0.5° at low latitudes to better resolve the equatorial wave guide. The model time step is 90 min and a free surface formulation is used (Roullet and Madec 2000).

The standard vertical resolution of ORCA2 is 10 m in the top 100 m increasing to 500 m at depth. However, B05 showed that to resolve 90% of the observed Dsst globally requires a vertical resolution in the upper ocean of 1 m or better and a temporal resolution of surface fluxes of 3 h or less. Guided by this study the number of vertical levels in the standard configuration has been increased by a factor of 10 producing a vertical resolution of 1 m in the top 100 m and giving a total of 301 levels. This approach of creating the high vertical resolution, or 'HRES', configuration has the advantage of preserving the same bathymetry as the standard configuration, thereby avoiding zeroth order sensitivity to variation of bathymetry in experiments at the HRES and standard vertical resolutions.

In the ORCA2 configuration used here there were no significant isuees with the model numerical behaviour. However it is recommended that use caution and care is taken in the implimentation of such a high vertical resolution.

2.2 Experimental design

Sections 3 and 4 present the validation of the diurnal variability of the high vertical resolution configuration ORCA2. The refined configuration resulting from the validation process is then used to perform two sensitivity experiments. FHDC (Forced High vertical resolution Diurnal Cycle) which explicitly resolves the diurnal cycle and FHDM (Forced High vertical resolution Daily Mean) which is identical to FHDC except that the surface fluxes of SWF are daily means, excluding the diurnal cycle.

All integrations start from the same initial condition which is the end of a 5 year spin-up from Levitus temperature and salinity at rest forced by a daily climatology of fluxes from ERA-40 (Simmons and Gibson 2000) with a linear feedback on the SST of –40 W m^{-2} K^{-1} toward the Reynolds product used in ERA-40. The linear feedback term is essential in climate time scale ocean integrations and is used through out all integrations. The necessity of the linear feedback term precludes any detailed assessment of the influence of the diurnal cycle on mixed layer temperature changes. This will require the coupled atmosphere experiments described in Part 2.

The behavior of FHDM was also compared to an integration with the same fluxes and physics but with the standard vertical resolution (31 levels). It was found that there were no significant differences in the upper ocean temperature, salinity or current structure when using daily mean fluxes. This is a re-assuring result in itself as it implies that the physics has converged and is essentially behaving in the same way in the HRES configuration as in the 31 level configuration.

Experiments are initially 1 year long to validate the diurnal variability and are then extended to 12 years.

2.3 Diurnal surface forcing dataset

In order to perform diurnally varying experiments in a global OGCM, a diurnally varying surface flux dataset is required. To construct a diurnal flux dataset a technique is used in which the diurnal cycle of SWF is reconstructed from daily mean values. This is done by assuming that the diurnal cycle of SWF is a scaling of the top of the atmosphere diurnal cycle of incident SWF. A global diurnal forcing dataset of SWF is then made at a 3 hourly resolution (see ''Appendix A'' for details) from ERA-40. Fluxes of longwave radiation, turbulent heat fluxes, freshwater and momentum are used as daily mean values from ERA-40. The equivalent daily mean flux data set is also made to perform sensitivity experiments. It is acknowledged that there are errors in surface fluxes from the ERA-40 reanalysis, which will be discussed in detail later, however as the aim of the present study is to perform sensitivity experiments these biases are deemed acceptable.

3 Validation of diurnal SST variability

For validating Dsst, there is the possibility of using one of a number of parameterizations of Dsst in the literature. These parameterizations can essentially be split into two types. The schemes of Webster et al. (1996) and Kawai and Kawamura (2002) are of the first type of parameterization which are 'model derived'. In these parameterizations a 1D mixed layer model is used to simulate in-situ measurements of the diurnal variability of SST, with the model being tuned to give the best agreement between the model and observations. The parameterization of Dsst is then derived from the model's sensitivity to surface fluxes assuming that the 1D model would perform equally as well in situations under which it has not been tested. Consequently using such a parameterization to validate modelled Dsst in the present study would at best produce very site specific (that of the observations used to tune the 1D model) intercomparison between two models and would be of limited practical use.

The parameterizations of Kawai and Kawamura (2003) and Gentemann et al. (2003) (second type) are derived from satellite measurements of Dsst. These parameterization are consequently based on much larger spatial domain compared with in-situ data. The large amount of data included in the derivation of such parameterisations covers many different oceanographic and meteorological conditions and, as such, provide better basis for the validation of global Dsst.

Of these two observational parameterizations mentioned above, Kawai and Kawamura (2003) is based on geostationary satellite data from the GMS/VISSR program covering a limited region off the coast of Japan and data from the SeaWinds instrument on QuikSCAT. The scheme of Gentemann et al. (2003) (GM03 from here on) is derived for data from the equatorial orbiting tropical rainfall measuring mission (TRMM) (Wentz et al. 2000) program and from the polar orbitting PathFinder (PF) satellite (Kilpatrick et al. 2001). In this study we will use the scheme of GM03 though comparisons with the scheme of Kawai and Kawamura (2003) (not shown) show that there is good agreement between the two.

The aim of GM03 is to develop a parameterization of Dsst so that biases due to incomplete sampling of the diurnal cycle can be systematically removed from satellite SST products. They use the daily mean SWF, local overpass time, daily mean windspeed (u) and the Reynolds SST product (Reynolds et al. 2002) to create a parameterization of Dsst. Their scheme consists of a time

varying component based upon the local time, to allow for the overpass time of the satellite, multiplied by a factor which is determined from the daily mean wind speed and SWF. Throughout this study, only the magnitude of Dsst, rather than the 'shape' of the Dsst, will be considered and comparisons are made against the daily maximums of the GM03 parameterization and its sensitivity to surface fluxes.

The empirical GM03 parameterization is fitted to both PF and TRMM data, but due to the larger spatial extent of the PF data (60°S–60°N rather than 40°S–40°N) the model is compared to the fit to the PF data. Though the PF data is based on infrared data and as such cannot see through clouds, the precession of the orbit during the 13 years of data results in a drift in the overpass times and produces a very dense sampling of the diurnal cycle. The use of PF parameterization rather than that from TRMM will be discussed again in Sect. 7. The GM03 parameterization of the magnitude of the Dsst in the PF data as a function of daily mean u and SWF is:

$$\begin{aligned} &\mathrm{Dsst}^{\mathrm{PF}}\left(\overline{\mathrm{SWF}},u\right) = 0.344 \\ &\left[\left(\overline{\mathrm{SWF}} - \mathrm{SWF}_0^P\right) - 1.444\times10^{-3}\left(\overline{\mathrm{SWF}} - \mathrm{SWF}_0^P\right)^2\right]\mathrm{e}^{-0.29u} \\ &\text{for } \ \overline{\mathrm{SWF}} \geqslant \mathrm{SWF}_0^P \end{aligned} \tag{1}$$

where $\mathrm{Dsst}^{\mathrm{PF}}$ is parameterized diurnal variability of SST (in °K) of the PF satellite, $\overline{SWF}$ and u daily mean SWF and windspeed, respectively, where the SWF is in W m^{-2} and u in m s^{-1}. $\mathrm{SWF}_0{}^P$ = 24 W m^{-2} and is the low SWF cut off (a constant of the empirical fit).

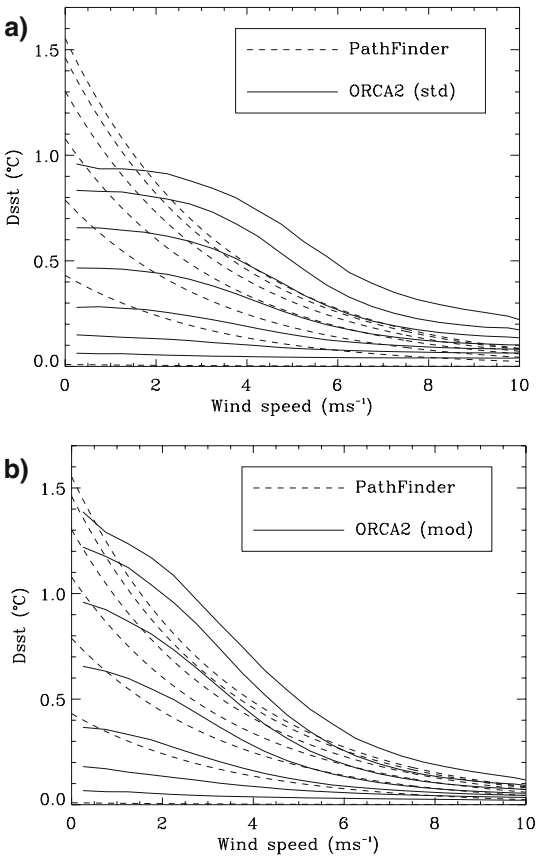

Fig. 2 Comparison of the Gentemann et al. (2003) parameterization of diurnal SST variability (*dashed lines*) and that produced by different configurations of a high vertical resolution OPA OGCM (*solid lines*). The configuration with no modifications is shown in **a**, while **b** shows the configuration where the back ground diffusivity is reduced and the Mellor and Blumberg (2004) parameterization of the effect of surface wave breaking on mixing is included. Each line is for a 50 W m^{-2} increment of daily mean SWF from 0 to 350 W m^{-2}

3.1 Modelled diurnal SST variability

Equation 1 is shown in Fig. 2a against the modelled Dsst as a function of wind speed for binned values of SWF from 0 to 350 W m^{-2} in bins of 50 W m^{-2}. The model data is appropriately weighted to reproduce a similar latitudinal coverage of the PF data, though this process was found to have little impact on the results. Figure 2a shows that over the entire range of SWF there is a lack of sensitivity of modelled Dsst to windspeed. There are two main features in this lack of sensitivity in the original HRES configuration of ORCA2. The first is that there is far too little diurnal variability in low wind speed conditions (<2 m s^{-1}), suggesting that there is too much mixing in the upper ocean in these conditions which is limiting the extent to which the daytime TBL shoals. The second discrepancy between the GM03 parameterization and the modelled Dsst is that there is too much Dsst in higher wind conditions (>7 m s^{-1}), suggesting conversely, that the model mixing scheme is not producing enough mixing in these conditions and consequently the TBL is too thin.

By examination of diagnostics of vertical mixing (not shown) it is found that the excessive mixing at low wind speeds was due to the numerical details of the model rather than to the physics of the TKE mixing scheme. Background vertical eddy viscosity and diffusivity of OPA are set globally to 10^{-4} and 10^{-5}, respectively, over the entire depth of the ocean and the effective vertical diffusivity is determined as the maximum of the background value or that produced by the vertical mixing scheme. However, in the equatorial eastern Pacific, the original version of OPA was prone to producing instabilities in the salinity field due to the advection scheme, leading to erroneous convection and a large cold bias. Consequently in the standard configuration, the background values are increased linearly over the top 40 m reaching ten times larger in the top layer to avoid these instabilities. Experimental runs where this

enhancement of the background values was removed (not shown) confirmed that the increase in these background values was responsible for the excessive near surface mixing and suppression of the Dsst during low wind periods.

To produce a more realistic diurnal cycle of mixing, and therefore SST, at low wind speeds whilst maintaining numerical stability, the advection scheme in OPA was changed to use a total variance dissipation (TVD) advection scheme (Levy et al. 2001). Though technically more diffusive, TVD requires far less explicit diffusion to maintain stability and so the background values may be maintained at their original values. It should be noted however that the errors produced by the original scheme where limited to the equatorial upwelling region of the Pacific. In areas other than these, the schemes performance is similar.

With regard to the discrepancy between the modelled Dsst and that of GM03 at higher wind speeds (Fig. 2a), Mellor and Blumberg (2004) (MB04 from here on) show that the Mellor-Yamada turbulence closure model (Mellor and Yamada 1974; Mellor and Yamada 1982) produces a much more realistic upper ocean thermal behavior when the effects of breaking surface waves are included. MB04 propose parameterization of the effects of surface wave breaking which in essence produces more efficient near surface turbulent mixing by increasing the surface boundary condition of TKE and introducing a dependence of near surface mixing length on the surface wave field. This is implemented here in OPA using a determination of 'wave age' from surface stress in the same manner as MB04.

The effect of the MB04 parameterization and reduced vertical background diffusion on the modelled diurnal cycle is shown in Fig. 2b. The diurnal cycle of upper ocean mixing and hence SST is improved. Low (high) wind speed Dsst is increased (decreased) by a factor of roughly 1.5.

B05 showed that in there idealized 1D modeling study that a vertical resolution of 1 m is needed near the surface to resolve Dsst. For completeness we repeated FHDC, with its modifications, at the standard 10 m vertical resolution. As anticipated this produced very little Dsst in line with the results in Figs. 10 and 12 of B05. These imply that just a handfull of extra near surface levels of 1 m resolution in OGCM would be required (as well as care over the physics) to resolve Dsst.

Now that the model is reproducing Dsst correctly, FHDC has been extended over the years 1985–1997. A seasonal climatology of Dsst from these 12 years is shown in Fig. 3. This climatology agrees well with the maps of Dsst produced from satellite data (Stuart–Menteth et al. 2003) and empirical parameterisations of Dsst (Clayson and Weitlich 2007) both in the spatial distribution and magnitude. There are many interesting features of this climatology. In DJF and MAM there is a large signal in the

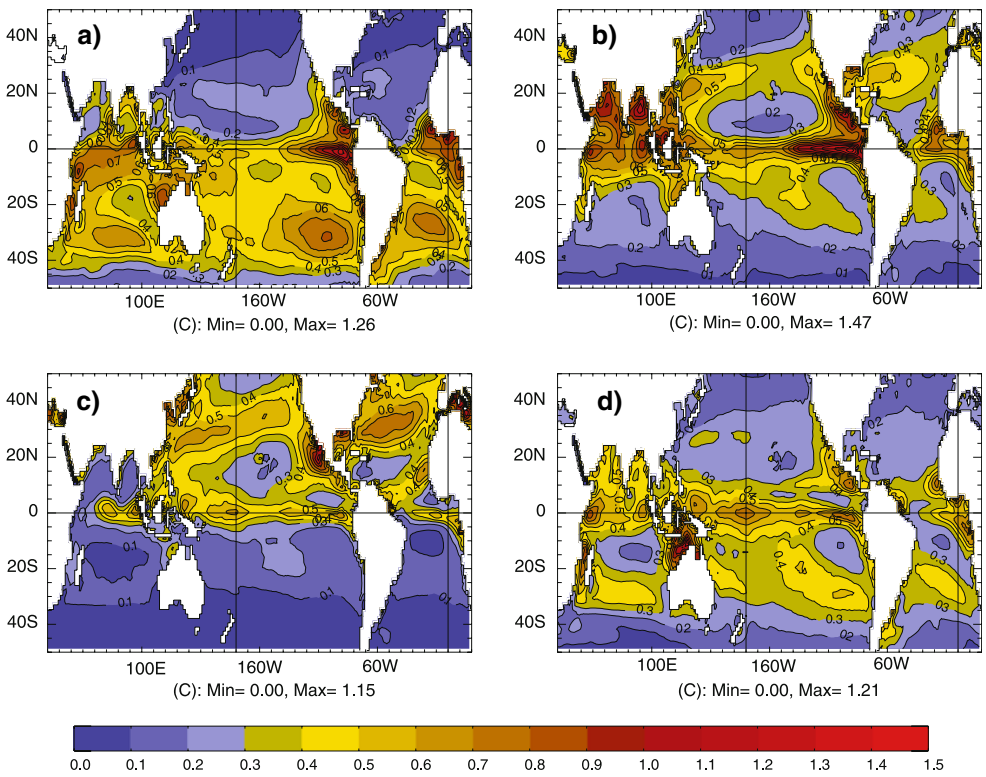

Fig. 3 Seasonal climatology of Dsst from a 12 year integration of FHDC, forced with daily mean fluxes except for a 3 h reconstructed diurnal cycle of short wave fluxes. Three-month means are shown for DJF (**a**), MAM (**b**), JJA (**c**) and SON (**d**)

equatorial eastern Pacific when the trade winds are light. Also in MAM there is a large Dsst in the northern Indian Ocean. This large climatological Dsst is this region increases the SST by around 0.4°. Such a warming is observed in this regions though coupled models are typically unable to capture this pre-monsoon warming and we suggest that this may be due to the absence of the diurnal cycle in such models.

4 Validation of diurnal current variability

As described previously, the left hand panel of Fig. 4 shows a week long composite of a diurnal jet from observations at the ocean station Papa during the LOTUS experiment. In order to show that the same process of diurnal cycling of upper ocean currents is present in FHDC, a similar composite is created from FHDC and is presented in the right hand panels of Fig. 4. However, though the composite is from the model grid point nearest to the location of the LOTUS mooring, there is very poor agreement between fluxes from ERA-40 used to force the model and the fluxes that were measured locally at the mooring. Consequently the composite shown in Fig. 4 is from a different time of year with weaker winds, approximately half the strength and depth, and smaller daily mean SWF. This period was chosen as it was a period in the ERA-40 data that exhibited relatively static conditions for a period of over a week. Although a direct comparison is not possible, the diurnal jet modelled in FHDC is in good qualitative agreement with that observed in the LOTUS data. The magnitude and depth scale of the modelled jet is about half that in the LOTUS composite. Nevertheless, it demonstrates that diurnal cycling of near surface currents due to the variation of mixing is similar to the observations.

A common feature of in-situ data is that the observed Ekman spiral (Ekman 1905) is flatter than predicted by Ekman's theory in that it decays in magnitude relative to its rate of rotation faster than in theory. PS99 examine this in a variety of 1D mixed layer models and find that the inclusion of the diurnal cycle leads to such a 'flattened' current spiral that is closer to observations than theory.

To examine the sensitivity of the time mean currents to the diurnal cycle FHDC is compared to FHDM. Hodographs of the mean currents from the initial 2 weeks of FHDC and FHDM are shown in Fig. 5, for a location near the LOTUS mooring, along with the decay rates of the magnitude and rotation rate of the currents with depth. The currents in FHDC are more surface 'trapped' and decay in

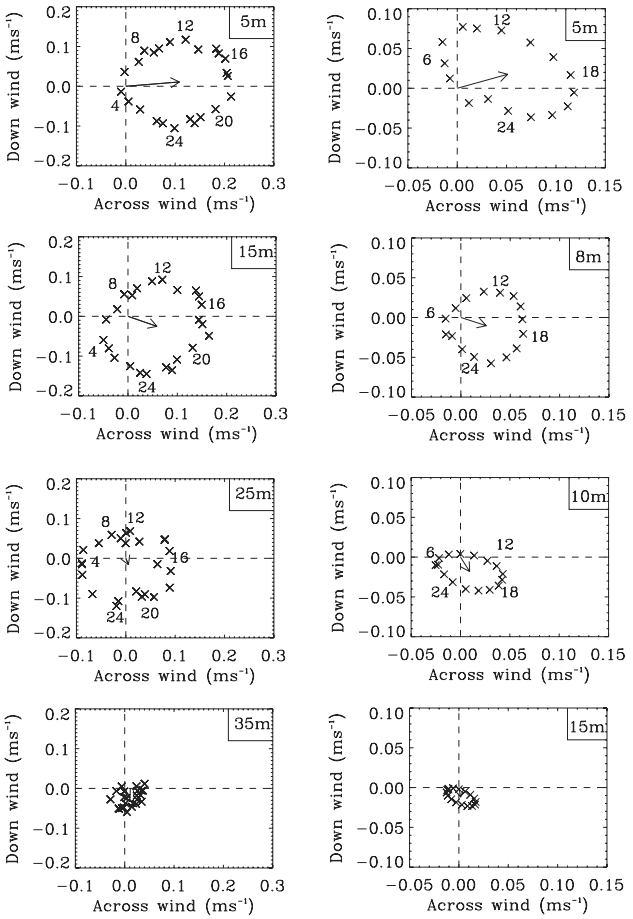

Fig. 4 *Left* Week long composite of current over the diurnal cycle from the LOTUS-PAPA mooring at 37°N, 70°W. Currents have been rotated into along and down wind directions and the numbers refer to the local time of day of the composited currents. *Arrows* show the mean current direction at each level. This plot is based on Fig. 9 from Price and Sundermeyer (1999). *Right* Same for FHDC and different surface forcing conditions. Note that the currents are at different depths

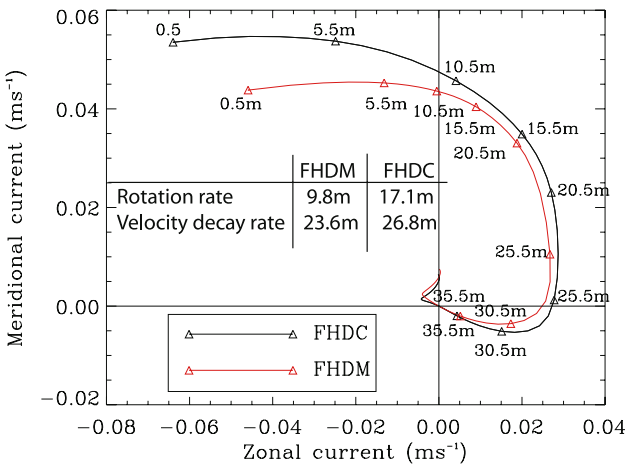

Fig. 5 Time mean Hodographs for FHDC and FHDM for first 9 days of the runs. Reference depth is 40 m and each 1 m depth is shown. Every 5 m a point is highlighted by a triangle to aid comparison

magnitude faster than they rotate. The ratio of these two decay scales is 1.6 times larger in FHDC than FHDM showing that the diurnal cycle is leading to a flattened spiral in the structure of the mean currents. This is slightly smaller than the factor of 2 found by PS99 but nonetheless demonstrates a similar effect.

5 Intraseasonal SST variability: response to the MJO

The aim of this section is to examine the intraseasonal SST variability across the tropical Indo-Pacific in FHDM and FHDC and assess to what extent the SST response to the MJO in enhanced by the inclusion of the diurnal cycle. Figure 6 shows a time longitude cross section of the intraseasonal SST variability averaged from 5°S to 5°N, at longitudes from 60°E east to the date line, during the TOGA-COARE period. Fig. 6a shows the SST from FHDM, Fig. 6b shows that from FHDC whilst Fig. 6c shows the difference in the SST from FHDC and FHDM. All the data in Fig. 6 is 3 hourly output and has been filtered with a 100 point 20–100 day bandpass Lanczos filter to leave only the intraseasonally varying component which is largely due to the passage of the MJO. In both FHDM and FHDC one can easily see the propagation of the SST signal from west to east in response to the different flux regimes of the MJO. The propagation of the active phase of the MJO (associated with a cooling of SST) is marked on Fig. 6. It is clear that the intraseasonal variability in FHDC is larger than in FHDM.

The SST difference between FHDC and FHDM (Fig. 6c) shows a good agreement between the periods where there is warming (cooling) in both experiments and where FHDC is warmer (cooler) than FHDM. This confirms, explicitly, the enhancement of the intraseasonal SST response to the MJO in the diurnally forced experiment FHDC. To demonstrate that the enhancement of the intraseasonal variability in FHDC is due to rectification by Dsst, Fig. 6d shows the filtered Dsst from FHDC. There is a quite good agreement between the difference in SST between FHDC and FHDM (Fig. 6c) and the Dsst (Fig. 6d) indicating that the increase in the intraseasonal response to the MJO is due to the Dsst.

We now examine the SST varability from FHDC and FHDM compared to observations from the WHOI-IMET mooring in the western Pacific warmpool. Figure 7 shows the SST from the WHOI-IMET mooring (a) and the SST from FHDC and FHDM (b) at the grid point nearest the mooring. Though there is a good agreement between the modelled SST from FHDC and the observed counterpart the Dsst is clearly often too small compared to observations, implying that any rectification of the intraseasonal variability is also underestimated. This is at first slightly

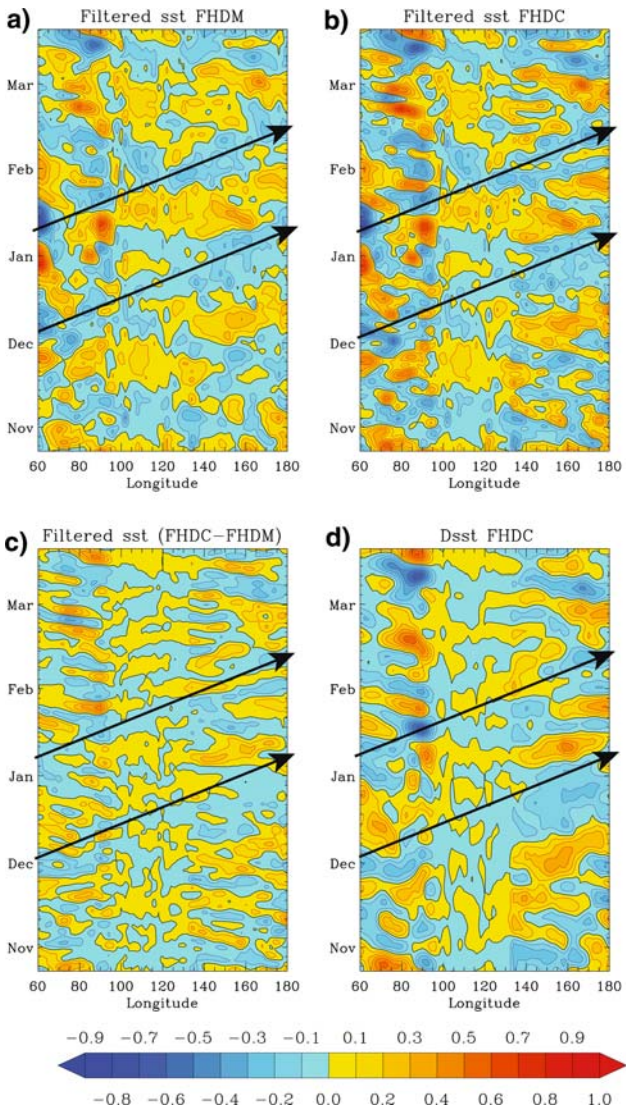

Fig. 6 Longitude-time plots from FHDM and FHDC for the TOGA-COARE period (November 1992–April 1993). Panels **a–c** show the SST averaged from 5°S–5°N for FHDM, FHDC and FHDC–FHDM. All data is based on daily mean data and has been 100 point 20–100 day Lanczos band pass filtered. Panel **d** shows the similarly filtered diurnal SST variability from FHDC averaged from 5°S–5°N. In each panel the propagation of the active phase of two strong MJO events are shown as *black arrows* to aid visual comparison

difficult to reconcile with the validation of the Dsst in Sect. 3 where the Dsst was apparently slightly too large compared to a satellite based parameterization (Fig. 2b), for low wind speeds. As is shown below, this discrepancy is due to the experimental design rather than the model physics.

B05 use a diagnosis of the diurnal and intraseasonal SST variability of the IMET time series (Fig. 7) to study various aspects of the modelled SST response to the MJO. Their diagnosis of Dsst was one standard deviation above the mean Dsst from the IMET time series. Their diagnosis of

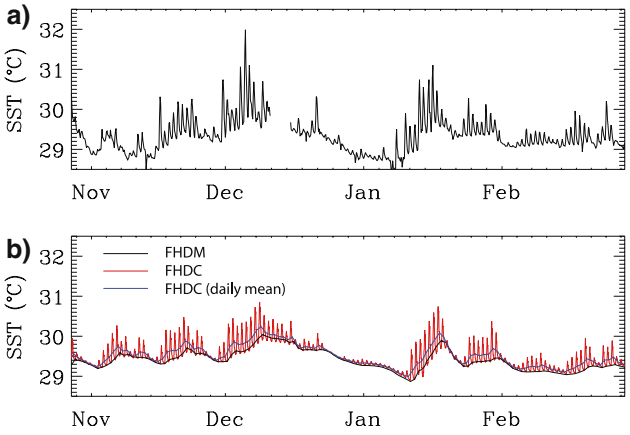

Fig. 7 Time series of SST during the intensive observing period of TOGA-COARE from observations (**a**) and modelled SST (**b**) from experiments FHDM (*black*) and FHDC (*red*) at the ORCA2 grid point nearest to the WHOI-IMET location. Also show is the running mean SST from FHDC (*blue*)

intraseasonal variability was the mean of each intraseasonal warming and subsequent cooling during the time series from a 3 day running mean filtered time series. The same simple diagnostics are used here to assess the impact of various parts of the experimental set up of FHDC and FHDM by use of a number of idealized experiments with a 1D version of OPA (Table 1). B05 show that a 1D KPP mixed layer forced by the observed hourly surface fluxes is able to capture over 90% of the diurnal and intraseasonal variability of SST. To ensure that the use of the TKE scheme has no impact on the results, a 1D experiment forced by the observed fluxes from TOGA-COARE with no feedback on the SST is performed (TKE-obs). The use of the TKE produced a change of the diagnosed Dsst from 0.95°C compared to 0.96°C in B05 (refereed to as KPP-obs in Table 1). Next, an experiment with the TKE scheme and forced by observations but at a 3 hourly temporal resolution rather than 1 h was performed called TKE-obs-3 h, again with no feedback on the SST. This produced a decrease in Dsst of about 10% in line with the findings of B05.

An additional experiment is performed (TKE-obs-3 h-FB), which uses the observed fluxes at a 3 hourly resolution but this time with the linear feedback on the model SST towards the SST from the nearest grid point of the Reynolds product used in ERA40, after interpolation onto the ORCA 2 grid. As the Reynolds product is based upon the spatial and temporally smoothed measurements of bulk mixed layer temperature there is little intraseasonal variability during the TOGA-COARE period and no diurnal variability. The Dsst is reduced further to 0.73°C compared to 0.86°C in TKE-obs-3 h, and the intraseasonal variability is also reduced. These changes are due to the Dsst being suppressed by the feedback on the SST. The intraseasonal variability is also reduced both due to the suppression of the Dsst and the reduction of the underlying mixed layer temperature variability itself, due to the feedback toward smoothed SST. In addition, as it has been shown previously that the Dsst indeed increases the intraseasonal SST variability in response to the MJO, the Reynolds product will always underestimate the intraseasonal variability due to its lack of diurnal variability.

Finally, a 1D experiment (TKE-era40-3 h-FB), is performed which uses the TKE scheme, 3 hourly fluxes with a reconstructed diurnal cycle of SWF (see appendix) and with a feedback on the SST toward the Reynolds product. The use of these surface fluxes further reduces the diurnal and intraseasonal SST variability by 11 and 4%, respectively). Consequently, the small Dsst and intraseasonal SST variability in FHDC (Fig. 7) is ascribed to the use of ERA-40 fluxes rather than observations and a linear feedback on SST toward a time series which underestimates variability and the temporal resolution of fluxes.

6 Mean dynamical structure of the tropical Pacific

Diurnal current variability has been shown to be qualitatively well modelled in Sect. 4. The impact of the diurnal vertical redistribution of momentum on the mean current structure of the tropical Pacific is now examined. Time mean zonal and meridional currents from the top model

Table 1 Summary of diagnosed diurnal and intraseasonal SST variability from 1D mixed layer models experiments with different flux resolutions and surface flux data sets

Experiment name	Forcing	Flux resolution	SST feedback	Diurnal SST variability	Intraseasonal SST variability
Kpp-obs	WHOI-IMET	1 h	No	0.96	0.84
TKE-obs	WHOI-IMET	1 h	No	0.95	0.83
TKE-obs-3 h	WHOI-IMET	3 h	No	0.86	0.78
TKE-obs-3 h-FB	WHOI-IMET	3 h	Yes	0.73	0.74
TKE-era40-h-FB	ERA-40	3 h	Yes	0.65	0.71

See text for details

level (1 m thick) from FHDM are shown in Fig. 8a and c, respectively. The difference in the mean surface currents between FHDC and FHDM are shown for zonal and meridional currents in Fig. 8b, d. The surface zonal currents are more westward by about 10% across much of the tropical Pacific. The meridional currents are also enhanced, with a clear signal of stronger divergence (10%) of surface currents along the equator. There is also an increase in the northward flow along the coast of South America towards the equator. The vertical velocity (Fig. 8e, f) shows that the increase in meridional divergence is associated with an increase in equatorial upwelling, implying a stronger shallow meridional overturning circulation or 'Ekman cell'.

The Ekman cell is the result of a balance between equatorial divergent wind driven transport in the upper ocean and a return flow at depth in a geostrophic equatorial convergence. The transport in the Ekman layer is governed by the wind stress and this transport is offset by turbulent mixing of momentum from the Ekman layer with the convergent geostrophic currents below. The windstress is equal in FHDC and FHDM while the heat fluxes differ only in the linear feedback term applied to the SST. As a consequence the transport in the Ekman layer is the same in FHDC and FHDM. Therefore, the differences can only originate from the different vertical redistribution of momentum by the diurnal cycle. In FHDC, the vertical redistribution of momentum by the diurnal cycle has modified the exchange of momentum between the upper ocean and the deeper ocean, resulting in a 10% stronger Ekman cell (Fig. 9).

7 Discussions and conclusions

A diurnal forcing data set is developed and then used to force a high vertical resolution (1 m) configuration of the OPA/ORCA2 OGCM. Comparison of the modelled Dsst to a satellite derived parameterization showed that the standard configuration of the high vertical resolution ORCA2 was unable to resolve the Dsst and its sensitivity to wind strength. Further examination showed that the near surface vertical diffusion, required for stability of the advection scheme, was unrealistically strong. By using a more stable

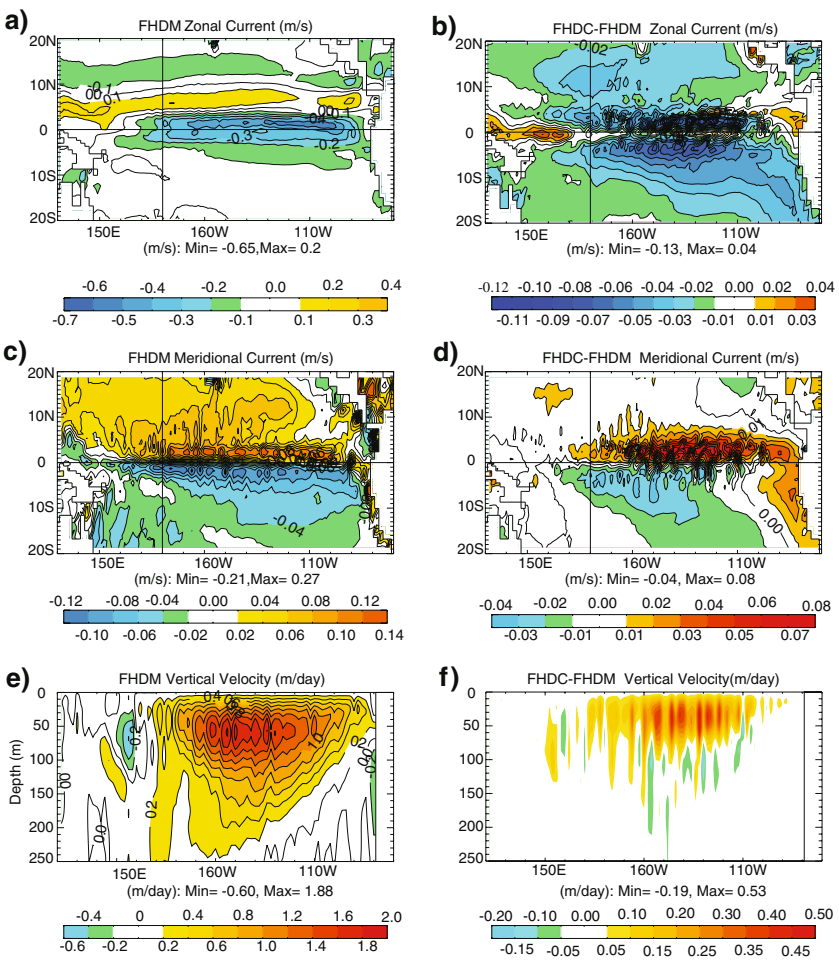

Fig. 8 Time mean currents from FHDC and FHDM. Panels **a** and **c** show the mean zonal and meridional currents, in the tropical Pacific, from the top model layer (1 m thick) of FHDM. Panels **b** and **d** show the difference in the zonal and meridional currents in the top model layer, again in the tropical Pacific, between FHDC and FHDM. Panels **e** and **f** show the time mean vertical velocity from FHDC and the difference between FHDC and FHDM with depth across the equatorial Pacific

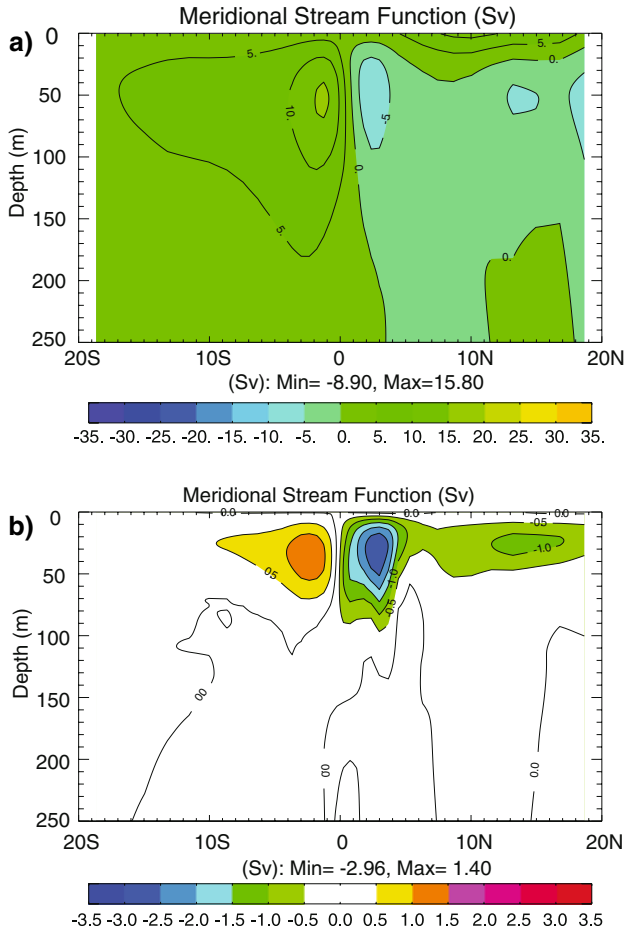

Fig. 9 Pacific meridional stream function for FHDM (**a**) and the difference between FHDC and FHDM (**b**)

advection scheme the near surface vertical background diffusivity was able to be reduced and the diurnal variability at low wind conditions was significantly improved, increasing by a factor of around 1.5 in low wind conditions (<2 m s^{-1}). It was also found that the addition of a parameterization of the effect of surface wave breaking on near surface mixing (Mellor and Blumberg 2004) improved Dsst in moderate wind conditions (>7 m s^{-1}) by generating more vertical mixing. These changes resulted in a model configuration which displayed a correct Dsst with an amplitude that reaches 2°C in regions of low wind stress and high insolation such as the Arabian sea, bay of Bengal and equatorial eastern Pacific during the boreal spring (see Fig. 3). It also produces a good qualitative representation of the diurnal jet and the 'flat' Ekman spiral that is seen in observations as documented by Price and Sundermeyer (1999).

A case study of the TOGA-COARE intensive observing period is performed and it is found, in line with the 1D modelling study of Bernie et al. (2005), that the diurnal cycle increases the intraseasonal SST variability across the Indo-Pacific warm pool by about 20% during this period. The result implies that the diurnal cycle is an important feature of ocean response to the MJO and it is proposed that along with the other model limitations discussed by Inness et al. (2003), the diurnal cycle is responsible for the too small intraseasonal SST variability in coupled models that otherwise produce a correct magnitude of surface flux variability associated with the MJO. How this affects the representation of the MJO in a coupled ocean–atmposphere GCM is addressed in Part 2 of this study.

The diurnal and intraseasonal SST variability during the TOGA-COARE period is seen to be smaller than observed and it is found that this is due to several factors. Firstly, as demonstrated by Bernie et al. (2005), the use of a 3 h temporal flux resolution instead of 1 h reduces the Dsst and, consequently, its rectification of the MJO signal. Furthermore the use of a linear feedback on the SST toward the Reynolds product is found to be a significant source of error for the modelled diurnal and intraseasonal SST variability as it contains very little intraseasonal variability and no diurnal variability. This is also related to the reduction in the diurnal and intraseasonal variability when using ERA40, as the reanalysis used this SST as a lower boundary condition. The implication is that future reanalysis products may be improved if a diurnal variability of SST is included in their lower boundary condition.

It is then shown that the inclusion of the diurnal cycle in an OGCM leads to a trapping of the atmospheric momentum fluxes near the surface in the time mean. This results in a flattened current profile compared to when no diurnal cycle is included. In the experiments presented here, the fluxes of momentum are identical and so we are able to attribute the difference in the current structures to differences in vertical mixing. The inclusion of the diurnal cycle leads to a reduction of mixing between the equatorial geostrophic convergence at depth and the equatorial divergence Ekman layer above. This results in Ekman cells which are about 10% stronger when the diurnal cycle is properly resolved.

There are a number of physical factors effecting the magnitude of Dsst that have not been explicitly addressed in the validation presented here. Firstly the effect of chlorophyll concentration on the absorption profile of SWF in the upper ocean has been neglected. However, sensitivity experiments (not shown) show that for realistic chlorophyll concentrations for the open ocean, chlorophyll concentration has little effect on the modelled diurnal SST variability, due to the absorption of the near infrared portion of the spectum (around 30% of the total) being unaffected by chlorophyll concentrations. This result supports the robustness of the validation even though a spatially homogeneous chlorophyll concentration is used in the experiments. It is worth noting that the 'traditional' Jerlov

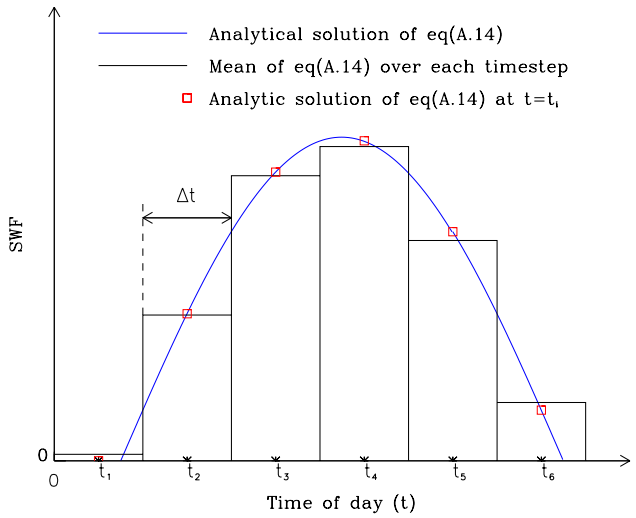

Fig. 10 Schematic to show graphically the implication of Eqs. 13 and 14; the mean value of the discrete solution is not the same as the analytic solution

(1976) profiles will provide a strong sensitivity as they are inappropriate for such high vertical resolution modelling as is presented here.

The seasonal variations of the diurnal cycle of SWF is also neglected in this study. Primarily this was due to its absence in the satellite derived parameterization used in the validation. For a given daily mean flux value, a high latitude summer diurnal cycle would produces a far lower peak solar flux than the same daily mean for a winter diurnal cycle at the same latitude. As the model developed here was able to resolve Dsst well, it was used to examine this further. It was found that the peak SWF was actually more important to the Dsst than the daily mean, with the shorter, higher peak, short wave winter days producing a higher Dsst for a given daily mean SWF than its summer counterpart. It is suggested that the use of the daily peak SWF, either in addition with or instead of the daily mean SWF, would improve the satellite derived parameterization used for validation. Indeed, the biases in the parameterization of Gentemann et al. (2003) are larger at higher latitudes, perhaps due to this effect. Furthermore, if the peak short wave flux is not available from the satellite data, it is proposed that the technique outlined in the appendix could be used to estimate it from the daily mean SWF.

Through changes in the SST via the Dsst and the dynamical impact of the diurnal cycle of mixing, the results presented here suggest that the diurnal cycle is a crucial component of the upper ocean heat budget and current system, but there are many restrictions in the issues that can be addressed due to the forcing set up used. The impact of the diurnal cycle on the mean state and variability of the tropical coupled ocean–atmosphere system is explored in the second part of this study, where the OGCM developed here is coupled to an AGCM.

Acknowledgments The authors are grateful for helpful discussions with Rowan Sutton and Pascale Delecluse as well as technical support from Jeff Cole D. Bernie and S. Woolnough were supported by NERC through grant NER/A/S/2000/1283. D. Bernie and G. Madec also acknowledge the support of the EU FP6 MERSEA project for this research.

Appendix A: Creation of diurnal forcing data

Reconstruction of diurnal cycle of short wave fluxes

(The IDL code for the following reconstruction of the diurnal cycle of SWF is available from the author on request.)

Daily mean data contains no information about the diurnal cycle of atmospheric convection or cloud cover. Consequently the reconstructed diurnal cycle of SWF is assumed to be simply be a scaling of the idealized top of atmosphere (TOA) incident SWF. If f is the function of the TOA SWF and t is time of day the basic assumption made can be expressed as:

$$\mathrm{SWR}_{\mathrm{rec}}(t) = S^* f(t) \tag{2}$$

where $\mathrm{SWF}_{\mathrm{rec}}$ (t) is reconstructed diurnal cycle of SWF and S^* is scaling factor. The value of S^* must be such that:

$$S^* \int_{\mathrm{dawn}}^{\mathrm{dusk}} f(t)\mathrm{d}t = \overline{\mathrm{SWF}}_{\mathrm{obs}}\mathrm{nspd} \tag{3}$$

where an over-bar represents a daily mean and nspd = 86,400 is the number of seconds per day. Reconstruction of the diurnal cycle of SWF ($\mathrm{SWF}_{\mathrm{rec}}$ (t)) will therefore require the determination of $f(t)$, its analytical integral and the limits of this integral so that S^* can be found by solving Eq. 3. A discrete version of Eq. 2 will then be used to reconstruct the diurnal cycle.

Diurnal cycle of top of atmosphere short wave fluxes

From some simple geometry the diurnal cycle of the top of atmosphere SWF can be derived as:

$$\begin{aligned} f(\phi,\theta,\delta,\mathrm{dss},t) = S_0[&\sin(\phi)\sin(\delta(\mathrm{dss})) \\ &+\cos(\phi)\cos(\delta(\mathrm{dss}))\cos(H_A(t,\theta))] \end{aligned} \tag{4}$$

where φ is latitude, θ longitude, δ declination of the earths orbit which is a function of dss the number of days since the winter solstice (21st December), S_0 TOA solar constant

and H_A, the ''hour angle'', is the angle due to the daily rotation of the earth. Here φ, θ, δ and H_A are all expressed in radians and that t refers to the time of day, in units of days, in the reference frame of the ERA-40 reanalysis (i.e., UTZ) and so will range from 0 to 1. Consequently:

$$H_A = (\theta + 2\pi t - \pi) \tag{5}$$

and

$$\delta = \left[\left(\frac{-23.5}{360}2\pi\right)\cos\left(\frac{\text{dss}}{\text{dpy}}2\pi\right)\right] \tag{6}$$

where dpy is number of days per year. The values in round brackets are to convert declination into radians and express the time of year as a fraction from 0 to 1.

Combining Eqs. 4, 5 and 6 gives a description of the diurnal cycle of the TOA SWF which depends upon longitude, latitude, time of day and time of year. However, this formulation will also produce negative values and so, as will be seen subsequently, care must be taken only to evaluate positive parts of $f(t)$ especially when considering its integral.

Analytical form and limits of integrated diurnal cycle of short wave fluxes

The integral of $f(t)$ is required to solve Eq. 3. Making the assumption that the declination (δ) is constant over any single (i.e., dss is constant) day and rewriting Eq. 3 for a single day as:

$$f(\phi,\theta,t) = (A + B\cos(C + Dt)) \tag{7}$$

where

$$\begin{aligned} A &= \sin(\phi)\sin(\delta) \\ B &= \cos(\phi)\cos(\delta) \\ C &= (\theta - \pi) \\ D &= 2\pi \end{aligned} \tag{8}$$

has the advantage that Eq. 7 can be integrated analytically to give:

$$\int_{\text{dawn}}^{\text{dusk}} f(\phi,\theta,t)\partial t = \left[At + \frac{B\sin(C + Dt)}{D}\right]_{\text{dawn}}^{\text{dusk}}. \tag{9}$$

All that now remains is to determine the limits of Eq. 9 such that Eq. 3 can be solved to find S^*. By solving Eq. 7 for $f(t) = 0$

$$\frac{\cos^{-1}(-A/B) - C}{D} = t_x \tag{10}$$

the solution, t_x, gives a time which the SWF will be zero i.e., either dawn or dusk. To determine which of these t_x represents the differential (Eq. 7) with respect to t is taken at $t = t_x$. A positive result indicating that t_x = dawn:

$$\begin{aligned} -BD\sin(C + Dt_x) > 0 \Rightarrow \quad t_x &= \text{dawn} \\ -BD\sin(C + Dt_x) < 0 \Rightarrow \quad t_x &= \text{dusk} \end{aligned}. \tag{11}$$

Now that either dawn or dusk has been found, the other limit can easily be found as the previous assumption that δ is constant over the course of a day produces a diurnal cycle which is symmetrical in time around midday (t_{md}). Therefore the difference in time between midday and either dawn or dusk allows one to easily find the other limit for Eq. 9 as t_{md} is solely a function of longitude:

$$t_{\text{md}} = 0.5 - \frac{\theta}{2}. \tag{12}$$

However Eq. 10 only has a solution when there is a distinct day and night, so at high latitudes where there is either 24 h of day or night then $|A| > |B|$ and Eq. 10 has no solution. If this is the case, then $A < B$ implies 24 h of night and so the integral in Eq. 8 is zero. Conversely $A > B$ implies a 24 h day and Eq. 8 should be integrated over the entire day by using the upper and lower limits of 1 and 0, respectively, in Eq. 9.

By using Eqs. 7, 8a–d, 9, 10,11a, b and 12 the limits of Eq. 9 can thus be found and this integral substituted into Eq. 3 to solve for S^*.

Reconstruction of discrete diurnal cycle

Analytically, having solved Eq. 3 for S^* the solution of Eq. 2 with Eq. 7 is trivial. However, to conserve $\overline{\text{SWF}}_{\text{obs}}$ in a reconstructed diurnal cycle over nts discrete steps requires that:

$$S^*\int_{\text{dawn}}^{\text{dusk}} f(t)\partial t = S^*\sum_{i=1}^{\text{nts}}\left(\int_{t_i-\Delta t/2}^{t_i+\Delta t/2} f(t)\partial t\right) = \overline{\text{SWF}}_{\text{obs}}\text{nspd}. \tag{13}$$

However at each time, t_i, Eq. 13 is not necessarily true as:

$$f(t_i)\Delta t \neq \int_{t_i-\Delta t/2}^{t_i+\Delta t/2} f(t)\,\partial t \tag{14}$$

where nts is required number of time steps per day, Δt length of the time step and t_i time at the centre of each time

step. Figure 10 shows graphically the significance of Eq. 14: the value of the analytical solution at $t = t_i$ (red squares) is not the same as the mean value of the analytic solution over a time step (black line). Consequently, the discrete solution for the reconstructed diurnal cycle should be calculated as

$$\mathrm{SWF_{rec}(t_i)} = \frac{\mathrm{S^* \int_{t_i-\Delta t/2}^{t_i+\Delta t/2} f(t)\partial t}}{\Delta \mathrm{t}}. \quad (15)$$

(Note that care should be taken not to integrate over any period where $f(t) < 0$). Using Eq. 15 rather than Eq. 2 will ensure that the following is satisfied and the reconstruction of the diurnal cycle conserves the total flux.

$$\frac{\sum_{i=1}^{\mathrm{nts}} \mathrm{SWF_{rec}(t_i)}}{\mathrm{nts}} = \overline{\mathrm{SWF}}_{\mathrm{rec}} = \overline{\mathrm{SWF}}_{\mathrm{obs}}. \quad (16)$$

Appendix B: List of acronyms

AGCM	Atmospheric general circulation model
B05	Bernie et al. 2005
CGCM	Coupled general circulation model
Dsst	Diurnal variability of SST
ERA-40	ECMWF re-analysis
FHDC	Forced OGCM experiments with high vertical resolution and a diurnal cycle of fluxes
FHDM	Forced OGCM experiments with high vertical resolution and daily mean fluxes
GCM	General circulation model
GM04	Gentemann et al. 2003
HRES	High vertical Resolution
IMET	Improved meteorological instrumenT
KPP	K-profile parameterisation [a first order turbulence closure vertical mixing scheme (Large et al. 1994)]
LOCEAN	Laboratoire d'Océanographie et de Climatologie par l'Expérimentation et l'Analyse Numérique (formerly LODYC)
LODYC	Laboratoire d'Océanographie Dynamique et de Climatologie
LOTUS	Long-term upper ocean study
MB04	Mellor and Blumberg 2004
MJO	Madden–Julian oscillation
OGCM	Ocean general circulation model
ORCA2	Two degree configuration of the OPA OGCM
OPA	''Océan Parallélisé''. Ocean model developed at (LODYC) in Paris (Madec et al. 1998)
PF	PathFinder
PS99	Price and Sundermeyer 1999
SST	Sea surface temperature
SWF	Short wave flux
TKE	Turbulent kinetic energy [a prognostic kurbulent kinetic energy vertical mixing scheme (Gaspar et al. 1990)]
TOA	Top of atmosphere
TOGA-COARE	Tropical ocean–global atmosphere-coupled ocean atmosphere response experiment
TRMM	Tropical rainfall measurment mission
TVD	Total variance dissipation

References

Anderson SP, Weller RA, Lukas RB (1996) Surface buoyancy forcing and the mixed layer of the western pacific warm pool: observations and 1D model results. J Clim 9:3056–3085

Bernie DJ, Woolnough SJ, Slingo JM, Guilyardi E (2005) Modelling diurnal and intraseasonal variability of the ocean mixed layer. J Clim 18(8):1190–120

Bernie DJ, Woolnough SJ, Guilyardi E, Slingo JM, Madec G, Cole J (2007) Impact of resolving the diurnal cycle in an ocean–atmosphere GCM. Part 2: diurnally coupled CGCM. Clim Dyn (submitted)

Blade I, Hartmann DL (1993) Tropical intraseasonal oscillations in a simple model. J Atmos Sci 50:2922–2939

Blanke B, Delecluse P (1993) Variability of the tropical Atlantic ocean simulated by a general circulation model with two different mixed-layer physics. J Phys Oceanogr 23:1363–1388

Briscoe MG, Weller RA (1984) Preliminary results from the long-term upper ocean study LOTUS. Dyn Atmos Oceans 8:243–265

Clayson CA, Weitlich D (2007) Variability of tropical diurnal sea surface temperature. J Clim 20:334–352

Ekman VW (1905) On the effect of the earths rotation on ocean currents. Ark Mat Astron Fys 2(11):1–53

Gaspar P, Grégoris Y, Lefevre JM (1990) A simple Eddy kinetic energy model for simulations of the oceanic vertical mixing: tests at station papa and long-term upper ocean study site. J Geophys Res 95(C5):16179–16193

Gentemann CL, Donlon CJ, Stuart-Menteth A, Wentz FJ (2003) Diurnal signals in satellite sea surface temperature measurments. Geophys Res Lett 30(3):1140

Inness PM, Slingo JM (2003) Simulation of Madden–Julian oscillation in a coupled general circulation model. Part 1: comparison with observations and an atmosphere-only GCM. J Clim 16:345–364

Inness PM, Slingo JM, Guilyardi E, Cole J (2003) Simulation of Madden–Julian oscillation in a coupled general circulation model. Part 2: the role of the basic state. J Clim 16:365–384

Jerlov NG (1976) Marine optics. Elsevier, New York

Johnson RH., Rickenbach TM, Rutledge SA, Ciesielski PE, Schubert WH (1999) Trimodal characteristics of troical convection. J Clim 12:2397–2418

Kawai Y, Kawamura H (2002) Evaluation of the diurnal warming of sea surface temperature using satellite derived marine meteorological data. J Oceanogr 58:805–814

Kawai Y, Kawamura H (2003) Validation of daily amplitude of sea surface temperature evaluated with a parametric model using satellite data. J Oceanogr 59:637–644

Kilpatrick KA, Podesta GP, Evans R.(2001) Overview of the NOAA/NASA advanced very high resolution radiometer Pathfinder algorithm for sea surface temperature and associated matchup database. J Geophys Res106(C5):9179–9198

Large WG, McWilliams JC, Doney SC (1994) Oceanic vertical mixing: a review and a model with a non-local boundry layer parameterization. Rev Geophys 32:363–403

Levy M, Estublier A, Madec G (2001) Choice of an advection scheme for biogeochemical models. Geophys Res Lett 28(19):3725–3728

Madec G, Delecluse P, Crepon M, Chartier M (1991) A three-dimensional numerical study of deep-water formation in the northwestern Mediterranean sea. J Phys Oceanogr 21(9):1349–1371

Madec G, Delecluse P, Imbard M, Lévy C (1998) OPA 8.1 ocean general circulation model reference manual. Institut Pierre-Simon Laplace (IPSL), Paris, No. 11

Mellor G, Blumberg A (2004) Wave breaking and ocean surface layer thermal response. J Phys Oceanogr 34:693–698

Mellor GL, Yamada T (1974) A hierarchy of turbulence closure models for planetary boundary layers. J Atmos Sci 31(1482):1791–1806

Mellor GL, Yamada, T (1982) Development of a turbulence closure model for geophysical fluid problems. Rev Geophys Space Phys 20:851–875

Morel A, Antoine D (1994) Heating rate within the upper ocean in relation to its bio optical state. J Phys Oceanogr 24(7):1652–1665

Price JF, Sundermeyer MA (1999) Stratified Ekman layers. J Geophys Res 104(C9):20467–20494

Price JF, Weller RA, Pinkel (1986) Diurnal cycling: observations and models of the upper ocean response to diurnal heating, cooling, and wind mixing. J Geophys Res 91(C7):8411–8427

Rajendran K, Kitoh A (2006) Modulation of tropical intraseasonal oscillations by ocean–atmosphere coupling. J Clim 19:366–391

Reynolds R, Rayner N, Smith T, Stokes D, Wang W (2002) An improved in-situ and satellite SST analysis for climate. J Clim 15(30):1609–1625

Roullet G, Madec G (2000) Salt conservation, free surface, and varying levels: a new formulation for ocean general circulation models. J Geophys Res 105(C10):23927–23942

Simmons AJ, Gibson JK (2000) The ERA-40 project plan. ERA-40 project rep. European Centre for Medium Range Weather Forcasting, UK

Slingo JM, Inness P, Neale R, Woolnough S, Yang G-Y (2003) Scale interactions on diurnal to seasonal timescales and their relevance to model systematic errors. Ann Geophys 46(1):139–155

Stommel H, Saunders W, Simmons W, Cooper J (1969) Observations of the diurnal thermocline. Deep Sea Res 16

Stuart-Menteth AC, Robinson IS, Challenor PG (2003) A global study of diurnal warming using satellite-derived sea surface temperature. J Geophys Res 108(C5):3155

Ward B (2006) Near-surface ocean temperature. J Geophys Res 111(C5):1–18

Webster PJ, Lukas R (1992) TOGA COARE: the coupled ocean–atmosphere response experiment. Bull Am Meteor Soc 73(9):1377–1416

Webster PJ, Clayson CA, Curry JA (1996) Clouds, radiation, and the diurnal cycle of sea surface temperature in the tropical western Pacific. J Clim 9:1712–1730

Wentz FJ, Gentemann CL, Smith DK, Chelton DB (2000) Satellite measurements of sea-surface temperature through clouds. Science 288(5467):847–850

Wijffels S, Firing E, Bryden H (1994) Direct Observations of the Ekman balence at 10N in the Pacific. J Phys Oceanogr 24:1666–1679

Woolnough SJ, Vitart F, Balmaseda MA (2007) The role of the ocean in the Madden-Julian Oscillation: implications for MJO prediction. Q J R Meteorol Soc 133:117–128

Zhang C, Dong M, Gualdi S, Hendon H, Maloney ED, Marshall A, Sperber K, Wang W (2006) Simulations of the Madden-Julian Oscillation in four pair of coupled and uncoupled global models. Clim Dyn 27(6):573–592